



# IGDB-2, an Ig/FNIII protein, binds the ion channel LGC-34 and controls sensory compartment morphogenesis in *C. elegans*

Wendy Wang, Elliot A. Perens<sup>1</sup>, Grigorios Oikonomou<sup>2</sup>, Sean W. Wallace, Yun Lu, Shai Shaham\*

Laboratory of Developmental Genetics, The Rockefeller University, 1230 York Avenue, New York, NY 10065, USA

## ABSTRACT

Sensory organ glia surround neuronal receptive endings (NREs), forming a specialized compartment important for neuronal activity, and reminiscent of glia-ensheathed synapses in the central nervous system. We previously showed that DAF-6, a Patched-related protein, is required in glia of the *C. elegans* amphid sensory organ to restrict sensory compartment size. LIT-1, a Nemo-like kinase, and SNX-1, a retromer component, antagonize DAF-6 and promote compartment expansion. To further explore the machinery underlying compartment size control, we sought genes whose inactivation restores normal compartment size to *daf-6* mutants. We found that mutations in *igdb-2*, encoding a single-pass transmembrane protein containing Ig-like and fibronectin type III domains, suppress *daf-6* mutant defects. IGDB-2 acts in glia, where it localizes to glial membranes surrounding NREs, and, together with LIT-1 and SNX-1, regulates compartment morphogenesis. Immunoprecipitation followed by mass spectrometry demonstrates that IGDB-2 binds to LGC-34, a predicted ligand-gated ion channel, and *lgc-34* mutations inhibit *igdb-2* suppression of *daf-6*. Our findings reveal a novel membrane protein complex and suggest possible mechanisms for how sensory compartment size is controlled.

## 1. Introduction

Animals require sensation to mount appropriate responses to environmental stimuli. Sensory organs detecting external cues are often comprised of glia, or glia-like cells, that form specialized compartments surrounding receptive endings of sensory neurons or neuron-like cells. Sustentacular cells in the olfactory epithelium, Deiters' cells in the cochlea, and retinal pigment epithelial cells in the retina are well-known examples of such compartment-forming glia-like cells (Bok, 1993; Breipohl et al., 1974; Rio et al., 2002). Sensory organ glia share several features with glial cells that surround excitatory synapses in vertebrate nervous systems. Both cell types express glial cell markers such as the intermediate filament protein GFAP, maintain extracellular ion and signaling molecule concentrations, engulf shed neuronal membranes, and exhibit complex intracellular calcium responses to upstream stimuli (Bok, 1993; Hansel et al., 2001; Hegg et al., 2009; Rio et al., 2002). Thus, understanding how sensory organ glia compartments arise and how they affect neuron receptive ending (NRE) functions, may shed light on activities of their central nervous system (CNS) counterparts (Shaham, 2010).

The nematode *C. elegans* provides a unique arena to study glia-neuron interactions, as developmental constraints allow neurons to survive even in the absence of glia (Bacaj et al., 2008). Glial loss or manipulation in this animal leads to profound sensory and/or synaptic deficits (Bacaj et al., 2008; Colón-Ramos et al., 2007; Felton and Johnson, 2011; Singhvi et al., 2016; Wallace et al., 2016). Importantly, interactions between single glia and neurons can be interrogated at the level of neuronal activity and animal behavior (Oikonomou and Shaham, 2011).

Each *C. elegans* possesses bilaterally symmetric anterior amphid sensory organs composed of 12 sensory neurons and two glial cells: a socket glial cell (AMso) and a sheath glial cell (AMsh) (Ward et al., 1975) (Fig. 1A). Eight amphid neurons extend ciliated dendrites anteriorly, passing through a matrix-filled tubular channel that opens to the environment (Perkins et al., 1986). AMso and AMsh glial membranes comprise the anterior and posterior sections of this channel, respectively, and are joined by tight junctions to form a continuous tube. Similar junctions attach glia to sensory neuron dendrites, sealing the posterior portion of the channel to form an isolated compartment surrounding ciliary NREs (Fig. 1B).

Amphid channel morphogenesis requires DAF-6, a Patched-related protein that restricts amphid channel expansion during

\* Corresponding author.

E-mail address: [shaham@rockefeller.edu](mailto:shaham@rockefeller.edu) (S. Shaham).

<sup>1</sup> Present address: 3020 Children's Way, MC 5137, San Diego, CA 92123, USA

<sup>2</sup> Present address: California Institute of Technology, Division of Biology, 1200 E. California Blvd., Pasadena, CA 91125, USA.

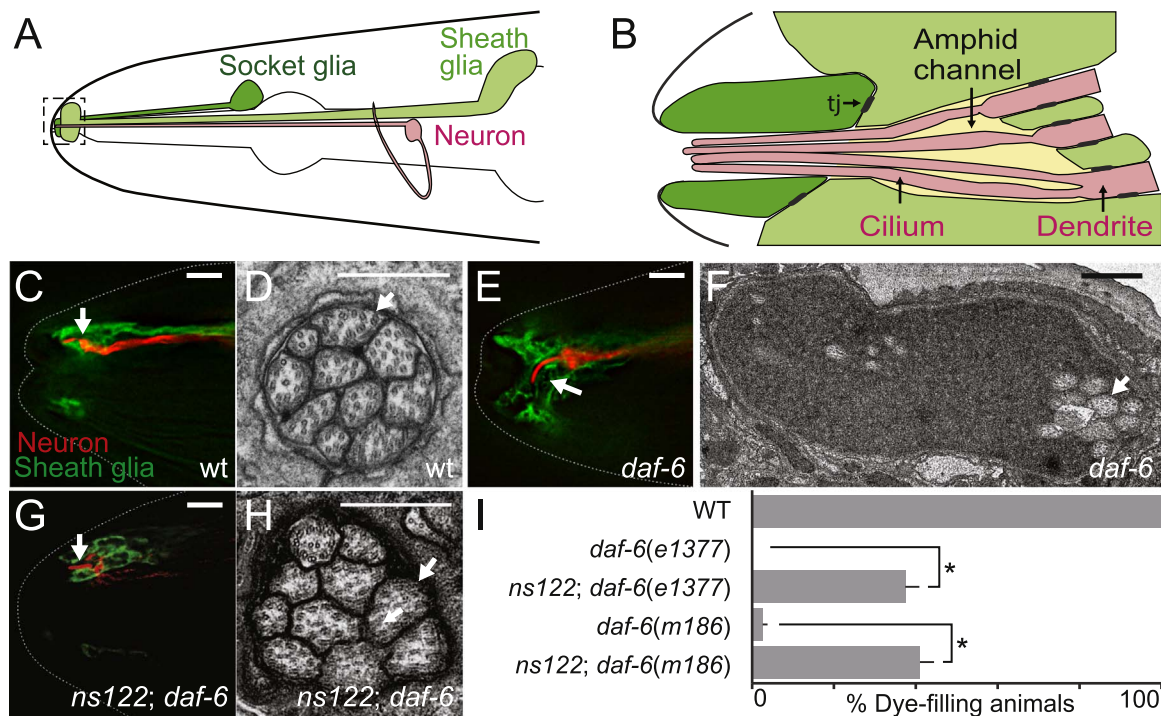


**Fig. 1.** *ns122* is a *daf-6* suppressor. (A) The *C. elegans* amphid consists of 12 amphid neurons (one is shown in red) and the sheath (light green) and socket glia (dark green). The amphid channel is outlined and shown in greater detail in (B). tj, tight junctions. (C, E, G) The amphid channel (white arrow) in wild-type (C), *daf-6(e1377)* (E), and *ns122; daf-6(e1377)* (G) adult animals. The ASER neuron is visualized with mCherry (red, driven by the *gcy-5* promoter) and the sheath glia with GFP (green, *T02B11.3* promoter). Left is anterior. Scale bar, 5  $\mu$ m. (D, F, H) Transmission electron micrographs of cross-sections through the amphid channel in wild-type (D), *daf-6(e1377)* (F), and *ns122; daf-6(e1377)* (H) adult animals. White arrows point to cilia. Scale bar, 0.5  $\mu$ m. Note the difference in scale in (F). (I) *ns122* suppresses *daf-6* dye-filling defects.  $n \geq 100$ . Error bars, standard error of the mean (SEM), from  $\geq 3$  experiments. \* $p < 0.0001$ . Adapted from Perkins et al. (1986).

development (Oikonomou et al., 2011; Perens and Shaham, 2005). Bloated channels in *daf-6* mutants can be restored to their proper size by mutations in either *lit-1* or *snx-1* genes (Oikonomou et al., 2012, 2011), suggesting that LIT-1, a Nemo-like kinase, and SNX-1, a retromer component, antagonize DAF-6 and promote channel growth. Indeed, *lit-1* mutants alone exhibit abnormally constricted channels. *daf-6*, *lit-1*, and *snx-1* also interact genetically with *che-14*, which encodes a Dispatched-related protein required for apical secretion from the AMsh glia (Michaux et al., 2000; Oikonomou et al., 2012, 2011; Perens and Shaham, 2005). DAF-6, LIT-1, and SNX-1 proteins all function in amphid glia, and localize to the amphid channel surface (Oikonomou et al., 2012, 2011; Perens and Shaham, 2005).

Here, we describe two novel regulators of amphid channel morphogenesis: IGDB-2, a single-pass transmembrane protein with Ig-like and fibronectin type III domains, and LGC-34, a predicted ligand-gated ion channel. We demonstrate that like *lit-1* and *snx-1* mutations, *igdb-2* mutations restore inappropriately expanded channels in *daf-6* mutants to their wild-type dimensions. IGDB-2 functions cell-autonomously in amphid glia, an activity requiring its N-terminal extracellular domain, and localizes to glial membranes forming the amphid compartment. *igdb-2* mutations also genetically interact with lesions in other components driving compartment expansion. LGC-34 binds IGDB-2 *in vivo* and in cell culture, and *lgc-34* loss suppresses *igdb-2* mutant defects. We suggest, therefore, that IGDB-2 promotes amphid channel expansion, in part, by antagonizing LGC-34 activity. Our studies identify a novel complex

controlling sensory compartment size, and suggest mechanisms for how compartment size may be regulated.

## 2. Materials and methods

### 2.1. *C. elegans* strains

Strains were cultured as previously described (Brenner, 1974). All animals were maintained and scored at 20°C for at least two generations without starvation. N2 animals were used as wild-type. Alleles in this study were: LGII *lgc-34(gk532, gk751837)*, LGIII *lit-1(ns132)* (Oikonomou et al., 2011), LGIV *igdb-2(ns122, gk214668)*, and LGX *snx-1(ns133)* (Oikonomou et al., 2012) and *daf-6(e1377, m186)* (Albert et al., 1981; Starich et al., 1995).

### 2.2. Identification of *igdb-2(ns122)*

SNP mapping was performed as described (Wicks et al., 2001). Briefly, CB4856 males were mated with *ns122; daf-6* hermaphrodites (N2 background). F2 recombinants were cloned, and F3 animals were scored for dye-filling as described in Section 2.6. SNP mapping placed *ns122* in the region between +4.96 and +6.44 on LG IV. Fosmid rescue experiments narrowed the mapping interval to map units between LG IV +5.97 and +5.98. Whole genome sequencing of the *ns122; daf-6* strain was performed, and the results analyzed using galign (Shaham, 2009). Mutations were found in two genes in the relevant interval: *igdb-2* and *T04A11.1*. Rescue studies confirmed *igdb-2* is the relevant gene.

### 2.3. Extrachromosomal arrays

The following arrays were used in this study: *nsEx5869*, *nsEx5870*, and *nsEx5884* ( $P_{T02B11.3}::GFP$  and  $P_{gcy-5}::mCherry$ ); *nsEx4695-nsEx4699* (WRM0629bG01 fosmid containing *igdb-2* and pMH135 ( $P_{pha-4}::GFP$ )); *nsEx4743-nsEx4747* (pWW3 and pMH135); *nsEx5663*, *nsEx5664*, and *nsEx5693* (pWW4 and  $P_{unc-122}::dsRed$ ); *nsEx5233-nsEx5236* (pWW5 and  $P_{unc-122}::dsRed$ ); *nsEx5436-nsEx5438* (pWW6 and  $P_{unc-122}::dsRed$ ); *nsEx5453-nsEx5456* (pWW7 and  $P_{unc-122}::dsRed$ ); *nsEx5373* (pWW8);  $Ex(pGT001(P_{itr-1}::GFP)$  and  $pRF4(rol-6(su1006))$ ) (Gower et al., 2001); *nsEx5189*, *nsEx5190*, *nsEx5192*, *nsEx5195*, and *nsEx5232* ( $P_{igdb-2}::IGDB-2(N\text{-terminal deletion})::GFP$  and  $P_{unc-122}::dsRed$ ); *nsEx5124*, *nsEx5125*, *nsEx5156*, and *nsEx5796* ( $P_{igdb-2}::IGDB-2(\text{middle deletion})::GFP$  and  $P_{unc-122}::dsRed$ ); and *nsEx5155*, *nsEx5157*, *nsEx5158*, and *nsEx5201* ( $P_{igdb-2}::IGDB-2(C\text{-terminal deletion})::GFP$  and  $P_{unc-122}::dsRed$ ).

### 2.4. Integrated arrays

The following arrays were used: *nsIs98* ( $P_{mir-228}::GFP$ ), *nsIs521* (pWW2 and  $P_{unc-122}::dsRed$ ), *nsIs355* (pWW1 and pRF4), and *sIs13244* ( $P_{lgc-34}::GFP$  and  $pCeh361(dpy-5(+))$ ) (McKay et al., 2003).

### 2.5. Plasmid construction

pWW3 consists of  $P_{igdb-2}::IGDB-2$  (genomic *SacI-XbaI* fragment from 5.4 kb upstream of ATG to 0.4 kb downstream of TAA, cloned into pBS). pWW4 was pBS containing  $P_{igdb-2}::IGDB-2(cDNA)::GFP$  with: 1) the same promoter fragment as pWW3, 2) the *igdb-2* cDNA amplified by polymerase chain reactions (PCR) from a mixed stage cDNA library, cloned into *NheI-AscI* sites, 3) GFP, and 4) *unc-54* 3'UTR. pWW5 consists of  $P_{mir-228}::IGDB-2(cDNA)::GFP$  ( $P_{mir-228}$  (Miska et al., 2007) cloned into *NotI-AscI* and *igdb-2* cDNA into *NheI-KpnI* sites in pSM-GFP). pWW6 and pWW7 are the same as pWW5 but with  $P_{itr-1}$  (2.1 kb) and  $P_{dyf-7}$  (1.8 kb) at *NotI-XmaI*, respectively (Gower et al., 2001; Heiman and Shaham, 2009). pWW8 is the same as pWW4, except with NLS-RFP fused to the *unc-54* 3'UTR, in place of  $P_{igdb-2}(cDNA)::GFP$ , cloned with *BamHI-MluI*. pWW9, pWW10, and pWW11 are the same as pWW4, but with the following cDNA deletion mutants:  $IGDB-2\Delta 25aa-784aa$ ,  $IGDB-2\Delta 786aa-1412aa$ , and  $IGDB-2\Delta 1441aa-1526aa$ , respectively. Plasmids used for worm co-immunoprecipitation studies were pWW1 and pWW2. pWW1 consists of  $P_{T02B11.3}::3xFLAG::GFP::LIT-1$  (inserted 3xFLAG into the *Acc65I* site in pG038) (Oikonomou et al., 2011). pWW2 consists of  $P_{igdb-2}::IGDB-2::GFP::3xFLAG$  (same as pWW3 but with  $GFP::3xFLAG$  fused to the 3' end of *igdb-2*, followed by the *unc-54* 3'UTR flanked by *Acc65I* sites). Plasmids used for cell culture co-immunoprecipitation studies were pWW12 (pLenti-CMV::LGC-34::GFP) and pWW13 (pLenti-CMV:: $IGDB-2::3xFLAG$ ), which were made using the Gateway® cloning system (ThermoFisher).

### 2.6. Dye-filling assay

Animals were washed off NGM plates into M9 buffer containing 10  $\mu\text{g}/\text{ml}$  diI (1,1'-diiododecyl-3,3',3'-tetramethylindocarbocyanine perchlorate) (ThermoFisher D282) and rotated at 20°C in the dark for 2 h. They were then transferred to new NGM plates and scored for dye-filling (animals with any subset of dye-filled amphid neurons were considered positive for dye-filling). For transgenic strains, at least three lines were scored and averaged. Statistical analysis of all dye-filling values was performed with the unpaired *t*-test (GraphPad), except for epistasis analysis which was performed with the one-way ANOVA test with Bonferroni's multiple comparisons (GraphPad).

### 2.7. Fluorescence and transmission electron microscopy

Images were acquired with a DeltaVision Image Restoration microscope (Applied Precision) with an Olympus UPLSAPO (60X, 1.3NA) silicone oil objective for amphid channel morphology and with an inverted TCS SP8 laser scanning confocal microscope (Leica) with a PlanApo (either 63x, 1.40NA or 100x, 1.46NA) oil objective for expression pattern studies. Deltavision images were deconvolved with SoftWoRx (Applied Precision). All fluorescence images were analyzed with ImageJ (NIH). For transmission electron microscopy, animals were sectioned and imaged as previously described (Perens and Shaham, 2005; Wallace et al., 2016).

### 2.8. Co-immunoaffinity purification from worms and mass spectrometry

Mixed stage worms were grown on peptone-enriched plates with HB101 bacteria, resuspended in homogenization buffer (50 mM HEPES-NaOH (pH 7.6), 1 mM EDTA, 150 mM NaCl, and 10% glycerol), and frozen as previously described (Mets and Meyer, 2009). Frozen worm powder was resuspended in homogenization buffer (with the addition of 1% NP-40 and Halt protease inhibitor (ThermoFisher 78429)), sonicated, and centrifuged at 20,000g for 15 min at 4°C. The supernatant (2–3 mg/ml, 5–10 ml total) was incubated with 200  $\mu\text{l}$  anti-FLAG® M2 affinity gel (Sigma A2220) for 2 h. Beads were washed 3 times with homogenization buffer and proteins eluted with SDS loading buffer. One third of the total eluate was resolved by SDS-PAGE (4–12% gradient) to one third the length of the gel, and stained with Coomassie Blue (BioRad 1610436). The protein was then in-gel trypsinized, and the extracted peptides were identified by MS/MS mass spectrometry (Rockefeller University Proteomics Resource Center). Western blot analysis was performed with anti-GFP (polyclonal rabbit, gift from Baolin Wang) and anti-FLAG® M2 (monoclonal mouse, Sigma F3165) at 1:1000, and HRP-conjugated donkey anti-rabbit and anti-mouse at 1:5000 (Jackson ImmunoResearch 711-035-152 and 711-035-150, respectively).

### 2.9. Cell culture and co-immunoaffinity purification

HEK293 cells were cultured in DMEM (ThermoFisher 11995065), supplemented with 10% heat-inactivated fetal bovine serum (Sigma F4135) and penicillin/streptomycin (ThermoFisher 15140-122). Transfections were performed using FuGENE HD (Promega E2311) according to the manufacturer protocol. Transfected cells were lysed with homogenization buffer and centrifuged at 20,000g for 10 min. The supernatant was incubated with either anti-FLAG® M2 affinity gel or anti-GFP, as was done with worm lysate (see above).

### 2.10. Expression profiling

mRNA expression profiling was described in Wallace et al. (2016). Unpublished data from those studies were mined for *igdb-2* and *lgc-34* expression levels.

## 3. Results

### 3.1. Mutations in *igdb-2* suppress sensory compartment morphogenesis defects of *daf-6* mutants

The amphid channel is a specialized sensory compartment, formed by the AMso and AMsh glial cells, through which sensory neurons extend cilia to access the external environment (Fig. 1B, C). These cilia are arranged in a stereotypical 3:4:3 pattern (Fig. 1D) and are tightly enveloped by the two glial cells. We previously showed that *daf-6* mutants, harboring lesions in the DAF-6 Patched-related protein,

exhibit a bloated channel containing excess extracellular material (Perens and Shaham, 2005). Within the bloated channel, neuronal cilia are disorganized and bent and fail to access the environment (Fig. 1E, F). The *daf-6* mutant defects suggest that this gene normally blocks channel expansion.

To identify genes that drive channel growth, we mutagenized *daf-6* mutants, and sought animals in which normal channel size is restored (see Oikonomou et al., 2011 for screen details). We previously described lesions in two genes, *lit-1*, encoding a Nemo-like kinase, and *snx-1*, encoding a retromer component, that suppress the *daf-6* mutant defect (Oikonomou et al., 2012, 2011). A third suppressor mutant, with allele designation *ns122*, was also found but not characterized.

To determine whether *ns122* indeed restores normal channel morphology to *daf-6* mutants, we examined *ns122; daf-6* double mutants carrying transgenes driving GFP expression in AMsh glia and mCherry in the ASER amphid sensory neuron. We found that the ASER cilium in the double mutant extends through a channel as in the wild type in 20% of animals ( $n=10$ , compare Figs. 1G to 1C, and note difference from 1E). To confirm these observations, we analyzed double mutants by transmission electron microscopy (TEM). As shown in Fig. 1H, the amphid channel indeed appears largely normal, with cilia tightly bundled and exposed to the environment ( $n=3$ , compare Figs. 1H to 1F; Fig. S1). However, cilia are not arranged in a 3:4:3 pattern, suggesting partial suppression.

To assess channel defects more quantitatively, we used a third assay. Some amphid neurons in wild-type animals can take up dyes, such as DiI, from the environment. Such dye uptake is blocked in animals in which sensory cilia fail to access the environment (Perkins et al., 1986). Consistent with our imaging assays, while neurons of *daf-6* mutants all fail to accumulate dye, 37% of *ns122; daf-6(e1377)* double mutants exhibit neuronal dye-filling in at least one of the two amphid sensory organs (Fig. 1I), confirming that *ns122* suppresses *daf-6* mutant defects. Crossing the *ns122* allele to another *daf-6* mutant, *m186*, results in a comparable dye-filling increase (Fig. 1I). Furthermore, three *ns122; daf-6(e1377)* animals that accumulated dye in only one amphid organ displayed only one amphid channel of more normal morphology by EM (Fig. S1), suggesting that dye-filling can serve to report on channel morphogenesis.

To identify the gene defective in *ns122* mutants, we used single nucleotide polymorphism (SNP) mapping and whole-genome sequencing to localize the *ns122* lesion to the *igdb-2* gene (Materials and methods), which encodes a single-pass transmembrane protein with multiple Ig-like and fibronectin type III (FNIII) domains (Fig. 2A). We found a Q579ochre mutation in *igdb-2(ns122)*

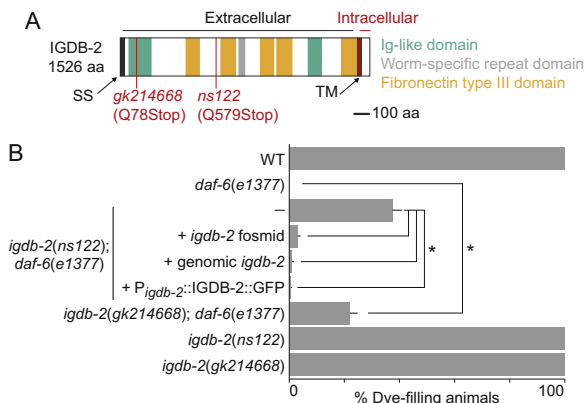


**Fig. 2.** *ns122* is an allele of *igdb-2*, which encodes an Ig/FNIII transmembrane protein. (A) Schematic of the IGDB-2 protein, marking truncations predicted in *ns122* and *gk214668*. SS, signal sequence. TM, transmembrane domain. (B) Dye-filling assay for indicated genotypes. Alleles used are: *daf-6(e1377)* and *igdb-2(ns122)*. (–) indicates no transgene.  $n \geq 87$ . Error bars, SEM, from  $\geq 3$  experiments. \* $p < 0.0082$ .

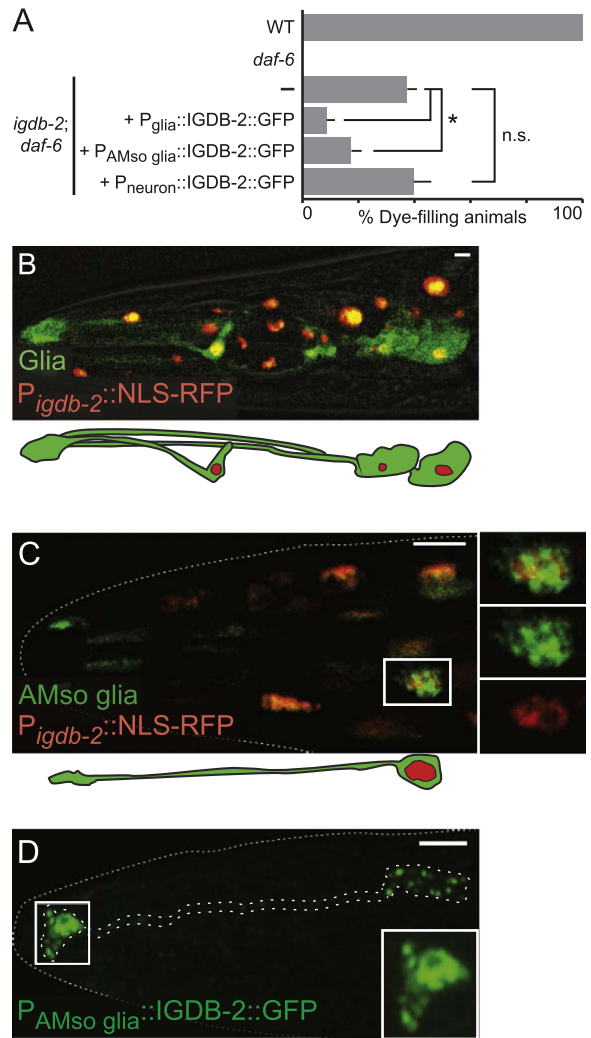


**Fig. 3.** *igdb-2* acts in and is expressed in glia to regulate amphid channel morphogenesis. (A) Dye-filling assay for indicated genotypes. Alleles used are: *daf-6(e1377)* and *igdb-2(ns122)*. (–) indicates no transgene. Promoters used for expression in glia, AMso glia, and neurons are  $P_{mir-228}$  (Miska et al., 2007),  $P_{itr-1}$  (Gower et al., 2001), and  $P_{daf-7}$  (Heiman and Shaham, 2009), respectively.  $n \geq 100$ . Error bars, SEM, from  $\geq 3$  experiments. \* $p < 0.0048$ , n.s. not significant. (B, C) Image of an adult (head) expressing  $P_{igdb-2}::NLS-RFP$  (red) and either (B)  $P_{mir-228}::GFP$  (in all glia, green) or (C)  $P_{itr-1}::GFP$  (in socket glia, green). Schematic of glia is shown below (B) and (C). (D) Adult expressing  $P_{itr-1}::IGDB-2::GFP$  (in socket glia, green). Outlined areas in (C) and (D) are shown in greater detail in inset. Scale bars, 5  $\mu$ m. Left is anterior.

mutants, leading to a predicted truncation of the IGDB-2 protein, preserving the first Ig and FNIII domains. To determine whether this *igdb-2* mutation is responsible for restoring wild-type channel shape to *daf-6* mutants, we crossed another *igdb-2* allele, *gk214668*, to *daf-6* mutants. This allele harbors a Q78ochre mutation and leaves only the first Ig domain intact (Fig. 2A). 22% of *igdb-2(gk214668); daf-6(e1377)* double mutants exhibit dye-filling, suggesting that *igdb-2* is indeed the relevant gene (Fig. 2B). Further supporting this conclusion, dye uptake in *igdb-2(ns122); daf-6(e1377)* mutants carrying an extrachromosomal array containing the *igdb-2* fosmid is reduced from 37% (no transgene) to 3% (Fig. 2B). Similarly, *igdb-2(ns122); daf-6(e1377)* mutants carrying a transgene containing the *igdb-2* genomic region (from 5.4 kb upstream of the start codon to 0.4 kb downstream of the stop codon) have reduced dye-filling (Fig. 2B); the same is true using the *igdb-2* promoter region to drive expression of an *igdb-2* cDNA::GFP fusion.

Together, these data demonstrate that lesions in *igdb-2* restore wild-type channel morphology to *daf-6* mutants.

3.2. *igdb-2* can act in AMso glia and localizes to sensory compartment membranes

To determine whether *igdb-2* functions in neurons or glia to regulate channel morphogenesis, we performed cell-specific rescue experiments. As shown in Fig. 3A, *igdb-2(ns122); daf-6(e1377)* mutants expressing an *igdb-2* cDNA::GFP fusion transgene under control of the glia-specific *mir-228* promoter, expressed during channel morphogenesis (Miska et al., 2007), have significantly reduced dye accumulation compared to non-transgenic animals. *igdb-2* cDNA::GFP expression in AMso glia alone, using an *itr-1* promoter fragment (Gower et al., 2001), also significantly reduces dye uptake. Importantly, *igdb-2* cDNA::GFP expression using the ciliated sensory neuron-specific *dyf-7* promoter, also active at the time of compartment morphogenesis (Heiman and Shaham, 2009), does not affect dye-filling of *igdb-2(ns122); daf-6(e1377)* mutants. Thus, *igdb-2* functions at least in part in AMso glia and not in neurons to regulate compartment shape.

The *igdb-2* gene expression pattern also supports this conclusion. Animals co-expressing *igdb-2* promoter::nuclear-RFP and glial *mir-228* promoter::GFP exhibit signal co-localization in glia, among other cells (Fig. 3B). A similar experiment using *itr-1* promoter::GFP to mark AMso glia, revealed co-localization with *igdb-2* promoter::GFP in these cells (Fig. 3C), consistent with our rescue studies.

To examine where IGDB-2 protein localizes within AMso glia, we generated animals carrying a transgene driving *igdb-2* cDNA::GFP expression in these cells. We found an enrichment of IGDB-2 near the amphid channel (Fig. 3D) and in vesicular structures in the cell body. This supports the notion that IGDB-2 is trafficked on vesicles to the amphid channel, where it participates in channel morphogenesis. These observations are consistent with previous findings demonstrating that DAF-6, LIT-1, and SNX-1 also localize to the amphid channel (Oikonomou et al., 2012, 2011; Perens and Shaham, 2005).

3.3. The IGDB-2 membrane-distal extracellular domain is required for compartment morphogenesis

The IGDB-2 protein consists of a large extracellular domain containing Ig-like and FNIII protein-protein interaction domains, as well as a short intracellular domain, which could be used for signal transduction. To uncover the functional significance of these domains, we generated *igdb-2(ns122); daf-6(e1377)* animals carrying transgenes in which the *igdb-2* promoter drives expression of truncated *igdb-2* cDNA::GFP proteins. As shown in Fig. 4, animals expressing IGDB-2ΔN::GFP, lacking membrane-distal extracellular sequences, exhibit dye accumulation comparable to non-transgenic mutants.

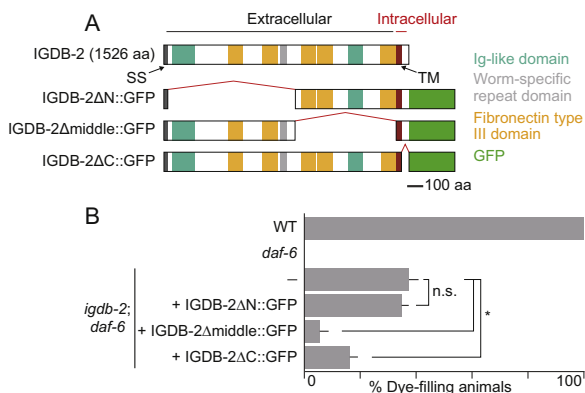


Fig. 4. The N-terminal membrane-distal domain of IGDB-2 is required for IGDB-2 function in amphid channel morphogenesis. (A) Schematic of wild-type and truncated IGDB-2::GFP proteins. (B) Dye-filling assay for indicated genotypes. Alleles used are: *daf-6(e1377)* and *igdb-2(ns122)*. (—) indicates no transgene.  $n \geq 100$ . Error bars, SEM, from  $\geq 3$  experiments. \* $p < 0.0024$ , n.s. not significant.

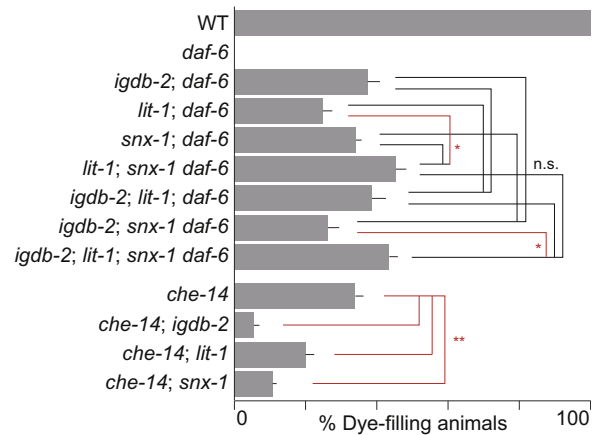


Fig. 5. *igdb-2* genetically interacts with other genes controlling compartment size. Dye-filling assay for indicated genotypes. Alleles used are: *daf-6(e1377)*, *igdb-2(ns122)*, *lit-1(ns132)*, *snx-1(ns133)*, and *che-14(ok193)*.  $n \geq 100$ . Error bars, SEM, from  $\geq 3$  experiments. n.s. not significant (black lines). \* $p < 0.019$  (red lines), by one-way ANOVA analysis with Bonferroni's multiple comparisons. \*\* $p < 0.0044$  (red lines), by unpaired *t*-test.

However, in mutants expressing either IGDB-2Δmiddle::GFP or IGDB-2ΔC::GFP, only 6% and 16% of animals take up dye, respectively, indicating that these transgenes remain functional. These results, therefore, indicate that the N-terminal membrane-distal domain of IGDB-2, containing one Ig domain, two FNIII domains, and a single nematode-specific repeat domain, is required for IGDB-2 channel morphogenesis functions, and that the membrane-proximal and intracellular domains are dispensable for activity. Thus, IGDB-2 is unlikely to function through intracellular signaling, and more likely influences compartment shape by interacting with extracellular moieties.

3.4. *igdb-2* genetically interacts with other genes controlling compartment size

Like *igdb-2* mutations, lesions in *lit-1* and *snx-1* only partially suppress *daf-6* mutant defects. One explanation for this is that more than one pathway drives compartment expansion; thus, disruption of a single pathway may not be sufficient to restore wild-type sensory channel morphology to *daf-6* mutants. We therefore sought to determine whether *igdb-2*, *lit-1*, and *snx-1* function in independent pathways. To this end, we generated the following triple mutants: 1) *lit-1*; *igdb-2*; *daf-6*, 2) *igdb-2*; *snx-1* *daf-6*, and 3) *lit-1*; *snx-1* *daf-6*. We then assessed their ability to take up dye, and compared them with the relevant *daf-6* double mutants. We found that 39%, 26%, and 45% of triple mutants accumulate dye in amphid sensory neurons, respectively (Fig. 5). Neither *lit-1*; *igdb-2*; *daf-6* nor *igdb-2*; *snx-1* *daf-6* mutants are statistically different from the corresponding double mutants, suggesting that *igdb-2* acts with *lit-1* and *snx-1*. However, *lit-1*; *snx-1* *daf-6* mutants show a significantly higher suppression (45%) than *lit-1*; *daf-6* mutants (25%), suggesting parallel functions for *lit-1* and *snx-1*, as previously reported (Oikonomou et al., 2012). However, this synergistic effect is much weaker than observed previously (Oikonomou et al., 2012), and not seen when comparing *lit-1*; *snx-1* *daf-6* mutants to *snx-1* *daf-6* mutants (34%). We speculate, therefore, that the differences from earlier findings may be due to background mutations in the double or triple mutants. Given the weakness of this synergy, and the lack of synergy between either *lit-1* or *snx-1* and *igdb-2*, these values together do not support parallel pathways for *lit-1*, *snx-1*, and *igdb-2*.

To verify this epistasis analysis, we generated *lit-1*; *igdb-2*; *snx-1* *daf-6* quadruple mutants. 44% of animals could take up dye, statistically comparable to the *lit-1*; *igdb-2*; *daf-6* and *igdb-2*; *snx-1* *daf-6*



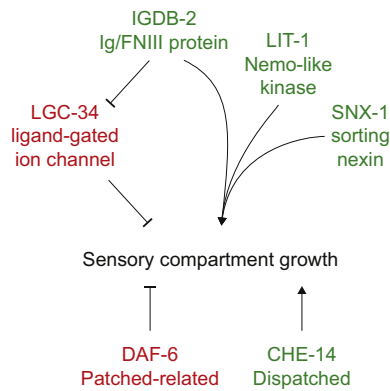


**Fig. 8.** A model for sensory compartment morphogenesis. IGDB-2 inhibits LGC-34, which in turn restricts sensory compartment expansion. IGDB-2 also independently promotes expansion, possibly with LIT-1 and SNX-1. DAF-6 restricts sensory compartment growth (Oikonomou et al., 2011), while CHE-14 promotes it (Michaux et al., 2000).

glial gene (Perens and Shaham, 2005), suggesting that LGC-34 and IGDB-2 are likely both expressed in glia.

### 3.6. LGC-34 restricts sensory compartment expansion and is inhibited by IGDB-2

To uncover possible *lgc-34* functions, we assessed whether *lgc-34* mutations affect amphid compartment morphology. *lgc-34(gk532)* contains a deletion spanning the *lgc-34* 5' UTR and the first 2 exons (Fig. 7A). We found that *lgc-34(gk532); igdb-2; daf-6* triple mutants had significantly reduced dye-filling, compared to *igdb-2; daf-6* double mutants (Fig. 7B). To confirm this, we crossed a second *lgc-34* allele, *gk751837*, predicted to generate a truncated protein with no transmembrane domains, into *igdb-2; daf-6* double mutants. The resulting triple mutant also displays a reduction in *igdb-2*-dependent *daf-6* suppression, with only 12% of triple mutants taking up dye. Neither *lgc-34* allele has a dye-filling defect on its own, and does not significantly restore dye-filling to *daf-6* mutants (Fig. S2). Thus, *lgc-34* appears to participate in amphid compartment morphogenesis downstream of *igdb-2*.

## 4. Discussion

### 4.1. A model for amphid compartment morphogenesis

The results presented here are consistent with a model in which *igdb-2* normally inhibits *lgc-34*, which in turn restricts sensory compartment growth (Fig. 8). Since *lgc-34* mutations do not fully suppress *igdb-2* mutant defects, *igdb-2* also likely functions independently, and perhaps together with *lit-1* and *snx-1* to influence amphid channel morphogenesis.

We also demonstrated that *igdb-2* functions, at least in part, in the AMso glia. This was somewhat surprising, given that *daf-6* is required in the adjacent AMsh glia to restrict amphid channel expansion (Perens and Shaham, 2005). Thus, *igdb-2* could be opposing *daf-6* in a paracrine manner, or both could be acting from both the AMso and AMsh glia. We favor the latter model based on the following observations. First, both *igdb-2* and *daf-6* are expressed in AMso and AMsh glia (Wallace et al., 2016; Perens and Shaham, 2005). Second, AMso glia-specific expression of *igdb-2* rescues *ns122* defects, but to a lesser degree than expression under the *igdb-2* or pan-glial *mir-228* promoter. This suggests that *igdb-2* may be acting from other cells, like the AMsh glia. Third, infrared laser-induced expression of *daf-6* in the AMsh glia in *daf-6* mutants restores dye-filling, but only in 30% of animals (Singhal and Shaham, 2017). Thus, *daf-6* function may similarly be required in the AMso glia, where it may function with IGDB-2.

### 4.2. IGDB-2 protein domains are found in other lumen-forming proteins

IGDB-2 contains Ig-like and FNIII domains, possibly providing insight into how the amphid channel forms. Ig/FNIII proteins are classified as cell adhesion molecule (CAM) members of the immunoglobulin superfamily, and play prominent roles in neurodevelopment (Sytnyk et al., 2017). A number of proteins with similar domains are specifically involved in lumen formation: Neogenin, a Netrin receptor in the zebrafish, promotes neural tube formation (Mawdsley et al., 2004); *Neuroglial*, the *Drosophila* L1-CAM homolog, promotes formation of glial canals of the antennal lobe (Chen and Hing, 2008); and Robo, the Slit receptor, promotes formation of astrocytic tunnels leading to the olfactory bulb in mice (Kaneko et al., 2010). Given that Neogenin, *Neuroglial*, and Robo all function as membrane receptors for cell-cell communication, IGDB-2 may function in a similar manner, directing communication between the AMso and AMsh glia, or between the glia and amphid neurons.

### 4.3. IGDB-2 binds LGC-34

Our findings suggest that IGDB-2 functions through LGC-34 to control amphid channel morphogenesis. What could be the functional nature of this interaction? One hypothesis is that IGDB-2 may alter membrane localization or stability of LGC-34. This scenario is reminiscent of how another Ig/FNIII transmembrane protein and Hedgehog coreceptor, Cdo, regulates activity of the Kir2.1 K<sup>+</sup> channel: Cdo forms a complex with Kir2.1 and increases cell surface expression of Kir2.1 in differentiating myoblasts (Leem et al., 2016). Notably, the *Drosophila* homolog of Cdo, Ihog (Interference hedgehog), forms a complex with Patched and a related Ig/FNIII protein, Boi (Brother of Ihog) (Zheng et al., 2010). This is intriguing given the genetic interactions we uncovered between *igdb-2* and *daf-6*, encoding a Patched-related protein. Moreover, Ihog interacts with Hedgehog *in vitro* and with Patched through its first and second FNIII domains (Zheng et al., 2010), respectively. Similarly, IGDB-2 structure-function analysis showed that the N-terminal membrane-distal domain, which contains its first two FNIII domains, is necessary for IGDB-2 function.

Alternatively, IGDB-2 may regulate the open/closed state of LGC-34, thus mediating ion flux across amphid glia, and possibly glial cell osmolarity. Consistent with this model, *igdb-2* lesions appear to enhance dye-filling defects of mutants carrying mutations in CHE-14, a Dispatched-related protein involved in osmoregulation and amphid channel morphogenesis (Michaux et al., 2000). Indeed, the expansion and contraction of the amphid channel could be consistent with changes in fluid accumulation and osmoregulation.

LGC-34 may also be gated by a specific ligand, since other LGC (ligand-gated ion channels of the *cys*-loop superfamily) proteins in *C. elegans* are neurotransmitter receptors. For example, LGC-55 is a tyramine-gated chloride channel expressed in head neurons and GLR glia, and likely functions in neurons to regulate head movements (Ringstad et al., 2009). In vertebrate glia, ligand-gated ion channels are known to activate downstream signaling cascades (Verkhatsky and Steinhäuser, 2000), providing possible clues for processes activated by LGC-34 and inhibited by IGDB-2.

Based on sequence analysis, LGC-34 is highly divergent from other LGCs as it has an atypical cysteine loop, normally involved in ligand-binding and present in most LGCs (Jones and Sattelle, 2008). Thus, it is also possible that LGC-34, along with IGDB-2, may be acting through a novel mechanism to regulate sensory compartment growth.

## Acknowledgements

We thank Shaham lab members for discussions and comments. We thank the Rockefeller University Proteomics and Bio-Imaging Resource Centers for technical support, and Baolin Wang and Howard Baylis for

reagents. Some strains were provided by the *Caenorhabditis* Genetics Center, which is funded by NIH Office of Research Infrastructure Programs (P40 OD010440). W.W. was supported by NIH Medical Scientist Training Program grant T32GM07739. S.S. was supported by NIH grants HD078703, NS064273 and NS081490.

## Appendix A. Supporting information

Supplementary data associated with this article can be found in the online version at doi:10.1016/j.ydbio.2017.08.009.

## References

- Albert, P.S., Brown, S.J., Riddle, D.L., 1981. Sensory control of dauer larva formation in *Caenorhabditis elegans*. *J. Comp. Neurol.* 198, 435–451.
- Bacaj, T., Tevlin, M., Lu, Y., Shaham, S., 2008. Glia are essential for sensory organ function in *C. elegans*. *Science* 322, 744–747.
- Bok, D., 1993. The retinal pigment epithelium: a versatile partner in vision. *J. Cell Sci. Suppl.* 17, 189–195.
- Breipohl, W., Laugwitz, H.J., Bornfeld, N., 1974. Topological relations between the dendrites of olfactory sensory cells and sustentacular cells in different vertebrates. An ultrastructural study. *J. Anat.* 117, 89–94.
- Brenner, S., 1974. The genetics of *Caenorhabditis elegans*. *Genetics* 77, 71–94.
- Chen, W., Hing, H., 2008. The L1-CAM, Neuroglian, functions in glial cells for *Drosophila* antennal lobe development. *Dev. Neurobiol.* 68, 1029–1045.
- Colón-Ramos, D.A., Margeta, M.A., Shen, K., 2007. Glia promote local synaptogenesis through UNC-6 (Netrin) signaling in *C. elegans*. *Science* 318, 103–106.
- Felton, C.M., Johnson, C.M., 2011. Modulation of dopamine-dependent behaviors by the *Caenorhabditis elegans* Olig homolog HLH-17. *J. Neurosci. Res.* 89, 1627–1636.
- Gower, N.J.D., Temple, G.R., Schein, J.E., Marra, M., Walker, D.S., Baylis, H.A., 2001. Dissection of the promoter region of the inositol 1,4,5-trisphosphate receptor gene, *itr-1*, in *C. elegans*: a molecular basis for cell-specific expression of IP<sub>3</sub>R isoforms. *J. Mol. Biol.* 306, 145–157.
- Hansel, D.E., Eipper, B.A., Ronnett, G.V., 2001. Neuropeptide Y functions as a neuroproliferative factor. *Nature* 410, 940–944.
- Hegg, C.C., Irwin, M., Lucero, M.T., 2009. Calcium store-mediated signaling in sustentacular cells of the mouse olfactory epithelium. *Glia* 57, 634–644.
- Heiman, M.G., Shaham, S., 2009. DEX-1 and DYF-7 establish sensory dendrite length by anchoring dendritic tips during cell migration. *Cell* 137, 344–355.
- Jones, A.K., Sattelle, D.B., 2008. The cys-loop ligand-gated ion channel gene superfamily of the nematode, *Caenorhabditis elegans*. *Invert. Neurosci.* 8, 41–47.
- Kaneko, N., Marín, O., Koike, M., Hirota, Y., Uchiyama, Y., Wu, J.Y., Lu, Q., Tessier-Lavigne, M., Alvarez-Buylla, A., Okano, H., Rubenstein, J.L.R., Sawamoto, K., 2010. New neurons clear the path of astrocytic processes for their rapid migration in the adult brain. *Neuron* 67, 213–223.
- Leem, Y.-E., Jeong, H.-J., Kim, H.-J., Koh, J., Kang, K., Bae, G.-U., Cho, H., Kang, J.-S., 2016. Cdo regulates surface expression of Kir2.1 K<sup>+</sup> channel in myoblast differentiation. *PLoS One* 11, e0158707.
- Mawdsley, D.J., Cooper, H.M., Hogan, B.M., Cody, S.H., Lieschke, G.J., Heath, J.K., 2004. The Netrin receptor Neogenin is required for neural tube formation and somitogenesis in zebrafish. *Dev. Biol.* 269, 302–315.
- McKay, S.J., Johnsen, R., Khattra, J., Asano, J., Baillie, D.L., Chan, S., Dube, N., Fang, L., Goszczynski, B., Ha, E., Halfnight, E., Hollebakk, R., Huang, P., Hung, K., Jensen, V., Jones, S.J.M., Kai, H., Li, D., Mah, A., Marra, M., Mcghee, J., Newbury, R., Pouzyrev, A., Riddle, D.L., Sonhammer, E., Tian, H., Tu, D., Tyson, J.R., Vatcher, G., Warner, A., Wong, K., Zhao, Z., Moerman, D.G., 2003. Gene expression profiling of cells, tissues, and developmental stages of the nematode *C. elegans*. *Cold Spring Harb. Symp. Quant. Biol.* 68, 159–170.
- Mets, D.G., Meyer, B.J., 2009. Condensins regulate meiotic DNA break distribution, thus crossover frequency, by controlling chromosome structure. *Cell* 139, 73–86.
- Michaux, G., Gansmuller, A., Hindelang, C., Labouesse, M., 2000. CHE-14, a protein with a sterol-sensing domain, is required for apical sorting in *C. elegans* ectodermal epithelial cells. *Curr. Biol.* 10, 1098–1107.
- Miska, E.A., Alvarez-Saavedra, E., Abbott, A.L., Lau, N.C., Hellman, A.B., McGonagle, S.M., Bartel, D.P., Ambros, V.R., Horvitz, H.R., 2007. Most *Caenorhabditis elegans* microRNAs are individually not essential for development or viability. *PLoS Genet.* 3, e215.
- Oikonomou, G., Perens, E.A., Lu, Y., Shaham, S., 2012. Some, but not all, retromer components promote morphogenesis of *C. elegans* sensory compartments. *Dev. Biol.* 362, 42–49.
- Oikonomou, G., Perens, E.A., Lu, Y., Watanabe, S., Jorgensen, E.M., Shaham, S., 2011. Opposing activities of LIT-1/NLK and DAF-6/patched-related direct sensory compartment morphogenesis in *C. elegans*. *PLoS Biol.* 9, e1001121.
- Oikonomou, G., Shaham, S., 2011. The glia of *Caenorhabditis elegans*. *Glia* 59, 1253–1263.
- Perens, E.A., Shaham, S., 2005. *C. elegans daf-6* encodes a Patched-related protein required for lumen formation. *Dev. Cell* 8, 893–906.
- Perkins, L.A., Hedgecock, E.M., Thomson, J.N., Culotti, J.G., 1986. Mutant sensory cilia in the nematode *Caenorhabditis elegans*. *Dev. Biol.* 117, 456–487.
- Ringstad, N., Abe, N., Horvitz, H.R., 2009. Ligand-gated chloride channels are receptors for biogenic amines in *C. elegans*. *Science* 325, 96–100.
- Rio, C., Dikkes, P., Liberman, M.C., Corfas, G., 2002. Glial fibrillary acidic protein expression and promoter activity in the inner ear of developing and adult mice. *J. Comp. Neurol.* 442, 156–162.
- Shaham, S., 2009. galign: a tool for rapid genome polymorphism discovery. *PLoS One* 4, e7188.
- Shaham, S., 2010. Chemosensory organs as models of neuronal synapses. *Nat. Rev. Neurosci.* 11, 212–217.
- Singhal, A., Shaham, S., 2017. Infrared laser-induced gene expression for tracking development and function of single *C. elegans* embryonic neurons. *Nat. Commun.* 8, 14100.
- Singhvi, A., Liu, B., Friedman, Christine, J., Fong, J., Lu, Y., Huang, X.-Y., Shaham, S., 2016. A glial K/Cl transporter controls neuronal receptive ending shape by chloride inhibition of an rGC. *Cell* 165, 936–948.
- Starich, T.A., Herman, R.K., Kari, C.K., Yeh, W.H., Schackwitz, W.S., Schuyler, M.W., Collet, J., Thomas, J.H., Riddle, D.L., 1995. Mutations affecting the chemosensory neurons of *Caenorhabditis elegans*. *Genetics* 139, 171–188.
- Sytnyk, V., Leshchynska, I., Schachner, M., 2017. Neural cell adhesion molecules of the immunoglobulin superfamily regulate synapse formation, maintenance, and function. *Trends Neurosci.* 40, 295–308.
- Verkhatsky, A., Steinhäuser, C., 2000. Ion channels in glial cells. *Brain Res. Rev.* 32, 380–412.
- Wallace, S.W., Singhvi, A., Liang, Y., Lu, Y., Shaham, S., 2016. PROS-1/prospéro is PROS-1/Prospero is a major regulator of the glia-specific secretome controlling sensory-neuron shape and function in *C. elegans*. *Cell Rep.* 15, 550–562.
- Ward, S., Thomson, N., White, J.G., Brenner, S., 1975. Electron microscopical reconstruction of the anterior sensory anatomy of the nematode *Caenorhabditis elegans*. *J. Comp. Neurol.* 160, 313–337.
- Wicks, S.R., Yeh, R.T., Gish, W.R., Waterston, R.H., Plasterk, R.H.A., 2001. Rapid gene mapping in *Caenorhabditis elegans* using a high density polymorphism map. *Nat. Genet.* 28, 160–164.
- Zheng, X., Mann, R.K., Sever, N., Beachy, P.A., 2010. Genetic and biochemical definition of the Hedgehog receptor. *Genes Dev.* 24, 57–71.